JAERI-M
5263

EXPERIMENTAL OBSERVATION OF COLLISIONLESS DRIFT WAVES IN THE JAERI TOROIDAL HEXAPOLE (JFT-1)

May 1973

Takashi NAGASHIMA, Harumi YAMATO*, Hideo OHTSUKA,
Tomio SHIINA, Sanae TAMURA and Shigeki ARIZONO

日本原子力研究所
Japan Atomic Energy Research Institute

JAERI-M 5263

Experimental Observation of Collisionless Drift Waves in the JAERI Toroidal Hexapole (JFT-1)

Takashi NAGASHIMA, Harumi YAMATO*, Hideo OHTSUKA, Tomio SHIINA, Sanae TAMURA and Shigeki ARIZONO

Nuclear Fusion Laboratory, Tokai, JAERI

(Received April 18, 1973)

Experimental study of low frequency waves has been made in a low β plasma of the JAERI toroidal hexapole with and without toroidal field. The observed waves are identified as density-gradient-driven collisionless drift waves and the interpretation of their mode transitions of poloidal mode number is given by comparison of the experimental results with the results predicted from the linear theory of a slab geometry.

* On leave from The Research and Development Center, Tokyo Shibaura Electric Co., Kawasaki, Japan.

JAERI－M 5263

原研トロイダル・ヘクサポール（ＪＦＴ－１）における無衝突ドリフト波の観測

日本原子力研究所東海研究所核融合研究室

永島　孝，大和春海*，大塚英男

椎名富雄，田村早苗，有薗重喜

（１９７３年4月１８日受理）

原研トロイダル・ヘクサポールに閉じ込められた低ベータ・プラズマ中の低周波波動についての実験的研究である。ヘクサポール磁場に，トロイダル磁場を重畳した場合と，しない場合とが調べられた。スラブ模型による理論結果との比較により，観測された波動は，密度勾配による無衝突ドリフト波であると同定された。また，ポロイダル・モード数の遷移についての物理的解釈がなされた。

＊　東芝総合研究所

CONTENTS

I. INTRODUCTION

The drift wave[1] is a fundamental mode of waves in a magnetically confined plasma. In the confined plasma the presence of spatial inhomogeneity of a plasma pressure is unavoidable. The importance of the drift wave is also derived from its causal relation to enhanced particle losses observed in low-β plasmas, i.e., losses above the lower limit set by classical binary-collision diffusion.

This type of instability was first predicted by Rudakov and Sagdeev,[2] and later by Krall and Rosenbluth[3] and by Mikhailovskaya and Mikhailovskii.[4] The theory of the drift instability was developed by Krall and Rosenbluth in complex field geometries[5] and by Rutherford and Frieman in general field configurations.[6] In the collisionless regime the drift wave is due to the interaction between the wave and resonant electrons moving along a magnetic flux line with velocities close to the phase velocity of the wave.

The present paper is concerned with experiments in the JAERI toroidal hexapole[7] which have demonstrated the existence of density-gradient-driven collisionless drift waves and their mode transition of poloidal mode number with the addition of a small toroidal field to the hexapole field. Section II of this paper describes the experimental parameters. Section III gives the experimental results. The identification of the wave and a mechanism of mode transition are discussed in Sec. IV.

II. PARAMETERS OF MACHINE AND PLASMA

Experiments to be described in the following sections have been carried out in a plasma confined in a toroidal hexapole field and the relevant machine parameters are summarized in Table I. The magnetic field of the hexapole is produced by three hoops internal to the plasma which are held in position by 4-mm-diam. rod supports (Fig. 1). The flux pattern is shown in Fig. 2. The hoops are energized by condenser bank of 28400 μF charged up to 3 kV. The quarter period of the hexapole field is about 8 msec. In the present experiment a charging voltage of the bank is at 0.5 kV. The separatrices are located at $\psi_S = 4.62 \times 10^{-3}$ and 4.63×10^{-3} Wb. The flux value of the stability limit line ψ_C is 4.25×10^{-3} Wb. The average hexapole field strength defined by $\langle B_p \rangle = \oint dl_p / (\oint B_p^{-1} dl_p)$ is 460 G on the stability limit line. The typical flux line in the fluctuation measurements is at the flux value of 4.39×10^{-3} Wb and passes through the point with the coordinates (40, 5.5) in Fig. 2. As shown in Fig. 3

I. INTRODUCTION

The drift wave[1] is a fundamental mode of waves in a magnetically confined plasma. In the confined plasma the presence of spatial inhomogeneity of a plasma pressure is unavoidable. The importance of the drift wave is also derived from its causal relation to enhanced particle losses observed in low-β plasmas, i.e., losses above the lower limit set by classical binary-collision diffusion.

This type of instability was first predicted by Rudakov and Sagdeev,[2] and later by Krall and Rosenbluth[3] and by Mikhailovskaya and Mikhailovskii.[4] The theory of the drift instability was developed by Krall and Rosenbluth in complex field geometries[5] and by Rutherford and Frieman in general field configurations.[6] In the collisionless regime the drift wave is due to the interaction between the wave and resonant electrons moving along a magnetic flux line with velocities close to the phase velocity of the wave.

The present paper is concerned with experiments in the JAERI toroidal hexapole[7] which have demonstrated the existence of density-gradient-driven collisionless drift waves and their mode transition of poloidal mode number with the addition of a small toroidal field to the hexapole field. Section II of this paper describes the experimental parameters. Section III gives the experimental results. The identification of the wave and a mechanism of mode transition are discussed in Sec. IV.

II. PARAMETERS OF MACHINE AND PLASMA

Experiments to be described in the following sections have been carried out in a plasma confined in a toroidal hexapole field and the relevant machine parameters are summarized in Table I. The magnetic field of the hexapole is produced by three hoops internal to the plasma which are held in position by 4-mm-diam. rod supports (Fig. 1). The flux pattern is shown in Fig. 2. The hoops are energized by condenser bank of 28400 μF charged up to 3 kV. The quarter period of the hexapole field is about 8 msec. In the present experiment a charging voltage of the bank is at 0.5 kV. The separatrices are located at $\psi_S = 4.62 \times 10^{-3}$ and 4.63×10^{-3} Wb. The flux value of the stability limit line ψ_C is 4.25×10^{-3} Wb. The average hexapole field strength defined by $\langle B_p \rangle = \oint dlp/(\oint B_p^{-1} dlp)$ is 460 G on the stability limit line. The typical flux line in the fluctuation measurements is at the flux value of 4.39×10^{-3} Wb and passes through the point with the coordinates (40, 5.5) in Fig. 2. As shown in Fig. 3

the hexapole field strength varies from 170 to 2290 G along the typical flux line and the average value is 438 G. L is a distance measured along the flux line from the nearest point to the symmetric axis. The radius of the curvature of the line R_c varies along the typical flux line as shown in Fig. 3.

In addition, a toroidal field is produced by a toroidal field coil (see Fig. 1). This produces a toroidal field component B_T perpendicular to the hexapole field B_P and the maximum strength is up to 1500 G at the minor axis. The field lines spiral around the current carrying hoops but the flux pattern in a poloidal plane is the same as that shown in Fig. 2. The toroidal field strength is measured as 44.2 I_T/R (G), where I_T (A) is the toroidal coil current and R (cm) is the major radius. The rotational transform angle $\iota/2\pi$ defined by $2\pi/\oint B_T/(RB_P)dlp$ once around the long way of the machine and the average shear length L_S defined by $(\iota/2\pi)^2 \int dl/\{(d\iota/d\psi)\int RB_P dl\}\Big|_\psi$ averaged along the flux line once around the minor axis are shown in Fig. 4 (a) and (b), respectively, as a function of the flux value for two toroidal fields (I_T = 22 and 45 A). Under the operating condition of I_T = 80 A the maximum shear parameter difined by $\textcircled{H} = 1/\kappa L_S$ is 3.7×10^{-3} ($\iota/2\pi$ = 15.4 and L_S = 130 cm) in the wall region where fluctuations are localized, where κ is the inverse density scale length $\nabla n_0/n_0$

The plasma is produced by the electron cyclotron resonance heating at a microwave frequency of 2.45 GHz in hydrogen gas. A short microwave pulse (500 μsec long) produces the plasma without preionization. Background neutral pressure of hydrogen is 6×10^{-5} Torr. The base pressure of the device is 4×10^{-7} Torr. Hereafter, most of experimental results are presented at 0.4 msec after the heating power is turned off. The peak density is 2×10^{10} cm^{-3} near the separatrices and the electron temperature T_e is 0.7 eV, which are determined from voltage-current characteristics of a floating double probe. Though the exact ion temperature T_i is unknown, a calculation of the ion heating by Coulomb collisions and the simultaneous cooling by charge exchange gives a value of ion temperature ~0.1 eV.

III. EXPERIMENTAL RESULTS

This section presents the experimental results of fluctuation measurements inside the $\oint dl/B$ stable region of the hexapole. There are two types of fluctuations, one in the frequency range of 15-35 kHz and 48-70 kHz in

the hexapole field strength varies from 170 to 2290 G along the typical flux line and the average value is 438 G. L is a distance measured along the flux line from the nearest point to the symmetric axis. The radius of the curvature of the line R_c varies along the typical flux line as shown in Fig. 3.

In addition, a toroidal field is produced by a toroidal field coil (see Fig. 1). This produces a toroidal field component B_T perpendicular to the hexapole field Bp and the maximum strength is up to 1500 G at the minor axis. The field lines spiral around the current carrying hoops but the flux pattern in a poloidal plane is the same as that shown in Fig. 2. The toroidal field strength is measured as 44.2 I_T/R (G), where I_T (A) is the toroidal coil current and R (cm) is the major radius. The rotational transform angle $\iota/2\pi$ defined by $2\pi/\oint B_T/(RBp)dlp$ once around the long way of the machine and the average shear length L_S defined by $(\iota/2\pi)^2 \int dl/\{(d\iota/d\psi)\int RBpdl\}\Big|_\psi$ averaged along the flux line once around the minor axis are shown in Fig. 4 (a) and (b), respectively, as a function of the flux value for two toroidal fields (I_T = 22 and 45 A). Under the operating condition of I_T = 80 A the maximum shear parameter difined by $\textcircled{H} = 1/\kappa L_S$ is 3.7×10^{-3} ($\iota/2\pi$ = 15.4 and L_S = 130 cm) in the wall region where fluctuations are localized, where κ is the inverse density scale length $\nabla n_0/n_0$

The plasma is produced by the electron cyclotron resonance heating at a microwave frequency of 2.45 GHz in hydrogen gas. A short microwave pulse (500 μsec long) produces the plasma without preionization. Background neutral pressure of hydrogen is 6×10^{-5} Torr. The base pressure of the device is 4×10^{-7} Torr. Hereafter, most of experimental results are presented at 0.4 msec after the heating power is turned off. The peak density is 2×10^{10} cm^{-3} near the separatrices and the electron temperature T_e is 0.7 eV, which are determined from voltage-current characteristics of a floating double probe. Though the exact ion temperature T_i is unknown, a calculation of the ion heating by Coulomb collisions and the simultaneous cooling by charge exchange gives a value of ion temperature ~0.1 eV.

III. EXPERIMENTAL RESULTS

This section presents the experimental results of fluctuation measurements inside the $\oint dl/B$ stable region of the hexapole. There are two types of fluctuations, one in the frequency range of 15-35 kHz and 48-70 kHz in

the laboratory frame with and without toroidal field, respectively, and another in the frequency range of 100-170 kHz in the laboratory frame and localized in the region of high field and locally bad curvature. The following observation is restricted to the former low-frequency fluctuation. Most of fluctuation measurements are performed using coaxially shielded spherical Langmuir probes 1 mm in diameter. The density fluctuation is estimated from the ion saturation current. The potential fluctuation is detected with a high impedance probe with a 200-kΩ resistor connected to the probe tip.

A. Distribution of Fluctuations

Typical scope traces of a density decay (the upper trace turned upside-down) and the density fluctuation triggered at 0.4 msec after the heating power is turned off are shown in Fig. 5 for two cases of (a) no toroidal field and (b) a small toroidal field of I_T = 10 A. Waveform of the fluctuation with and without toroidal field is seen to be almost sinusoidal. The observed frequency of the fluctuation is reproducible within 15 %. Its amplitude, however, is less reproducible and varies by a factor of 2-4, which is partly because the fluctuation is in a state of large amplitude and sometimes of amplitude modulation. As seen from the photograph the frequency of the fluctuation becomes lower in time and it is found to decrease with about the same decay constant as the product of κT_e.

Radial profiles of density and its fluctuation are shown in Fig. 6 with (a) no toroidal field and (b) the toroidal field of I_T = 10 A. The fluctuations with and without toroidal field are localized near the region of the maximum density gradient towards the walls with $\nabla n_0 / n_0 = 3.2$ cm^{-1} averaged along the typical flux line as $\oint \{|\nabla\psi|\ (d/d\psi) \ln n_0\} dl/B / \oint dl/B$. The amplitude is found to be almost uniformly distributed along the typical flux line regardless of the curvature of the line. This mode of fluctuation does not exist on the internal portion of the density gradient towards the hoops. The electron temperature gradient $\nabla T_e/T_e$ is measured to be smaller than the density gradient by a factor of 7-10. The average ion Larmor radius ρ_i is 1 mm.

B. Frequency and Propagation Direction of Waves

The observed frequency in the laboratory frame are shown in Fig. 7

as a function of toroidal field. With the addition of B_T to the hexapole field the frequency decreases by a factor of 2-3 and frequency jumps are observed beyond the critical toroidal fields. In each branch of three curves the frequency is found to be nearly held constant or slightly lowered. The frequency of the wave in the plasma rest frame is in the range of 19-39 kHz and 59-85 kHz with and without B_T, respectively, after a correction of $\vec{E}_0 \times \vec{B}$ rotation due to a radial electric field $\vec{E}_0$ estimated from the floating potential and electron temperature profiles. The Doppler shift of the frequency is less than 30 %. The curvature drift velocity is negligible in the correction because the average velocity is found to be at most 2×10^4 cm/sec. The direction of propagation after the correction is also in the direction of the electron dimagnetic drift velocity. The ratio of the frequency in the plasma frame to the ~~electron diamagnetic~~ frequency ω/ω_{*e} lies in the range of 0.5-0.8 and 0.7-0.9 with and without toroidal field, respectively.

C. Phase difference between Density and Potential Fluctuations

The phase difference Δ_φ between density $\tilde{n}$ and potential $\tilde{\phi}$ fluctuations are measured with a Langmuir probe and a high impedance probe parallel to the typical flux line. It is observed that the density wave is leading by 94 ± 51 and 71 ± 51 degrees with and without toroidal field, respectively. We note that the relative amplitude for potential $e\tilde{\phi}/KT$ and density $\tilde{n}/n_0$ fluctuations ~~are~~ equal within a factor of 2, as expected from an electrostatic mode (here, $\beta \simeq 4 \times 10^{-6}$).

D. Determination of Parallel and Perpendicular Wavenumbers and Mode Transitions

The spatial properties of the wave are investigated by measuring the relative phase difference of probe signals at various positions. The correlation in the direction of the density gradient is good and no phase shift is observed. Figure 8 shows the azimuthal wavelength λ_θ in the direction perpendicular to both the magnetic field and the density gradient. Three branches of curves are obtained with the addition of B_T to the hexapole field.

Poloidal mode number n is obtained from the phase measurements using three probes on the same flux line. Probes are positioned within 1 mm on the line in given a poloidal plane at fixed azimuth using a narrow electron

beam. In Fig. 9 we plot the positions of the maxima of the waveform as shown in Fig. 5 as a function of time delay in the case of no toroidal field. The slope of a given line gives the parallel phase velocity of the wave in the laboratory frame ($3.2\text{-}3.5 \times 10^6$ cm/sec). It is also shown that the wave is a travelling wave and the poloidal mode number is n = 1 which also means that the parallel wavelength $\lambda_{\parallel}$ ($= 2\pi/k_{\parallel}$) is equal to the length of the closed flux line L_0 (= 80 cm). Similarly, poloidal mode number in each branch of curve shown in Fig. 8 with toroidal field is found to be held constant and in shown to be successively n = 0, -1, and -2 with increasing toroidal field. These mode transitions also correspond to the jumps of the frequency as observed in Fig. 7. Only in the mode transition regions two separate modes are detected as in a Q-machine plasma.[8,9]

Assuming a perturbed potential $\tilde{\phi} = \phi_1 \exp(ik_{\perp}s + ik_{\parallel} l - i\omega t)$, we can define the parallel and perpendicular wavelengths, respectively, as

$$k_{\parallel} = \frac{2\pi}{\int dl}\left(\frac{l_\theta}{\lambda_\theta} + n\right), \tag{1}$$

and

$$k_{\perp} = \frac{2\pi}{\int dl}\left(\frac{R\int R^{-1} dl_p}{\lambda_\theta} - \frac{l_\theta}{L_0} n\right), \tag{2}$$

where l_θ is a pitch length of the flux line defined by $l_\theta = \int B_T/B_p dl_p$; dl_p is the poloidal line element and dl is the line element along the flux line. Integrations are carried out along the line once around the minor axis. Strictly speaking, $k_{\perp}$ is replaced by $\sqrt{k_{\perp}^2 + k_r^2}$. However, since the radial wavenumber k_r is estimated from the radial amplitude distribution as 0.6 cm^{-1}, the error due to neglect of k_r is 5-20 %. The pitch length is measured using the electron beam as (Fig. 10)

$$l_\theta = (0.1933 \pm 0.0045) I_T + (0.15 \pm 0.10), \tag{3}$$

while the theoretical relationship is $l_\theta = 0.17\ I_T$. This result may suggest the presence of a small error field in the toroidal direction.

The parallel and perpendicular wavelengths are determined from Eqs. (1), (2), and (3) as shown in Fig. 11 (a) and (b), respectively, as a function of toroidal field. Three branches of curves are accompanied with the transitions of poloidal mode number when the toroidal field is superimposed on the hexapole. It is also found that the ratio of the

parallel wavenumber to the perpendicular wavenumber lies in the order of 10^{-2}. Figure 11 (c) shows amplitude of the density fluctuations as a function of toroidal field. It seems that large amplitude of the waves corresponds to small parallel wavenumber and large perpendicular wavenumber at least in the case of small toroidal fields. These wave behaviours with increasing the toroidal field will be well understood on the $(\lambda_{\parallel}\kappa, k_{\perp}\rho_i)$ plane as shown in Fig. 12. Also shown are the stable and unstable regions of a collisionless drift wave and contour lines of its constant growth rate, $\gamma = \omega_I/\kappa v_{thi}$, for $T_e/T_i = 10$ and $\nabla T_e = 0$ calculated by Brossier,[10] where ω_I is the imaginary part of the frequency and v_{thi} is the ion thermal velocity. Without toroidal field (the solid dot in the figure) the observed parallel wavelength of the n = 1 mode is the longest one because it must be L_0/n from geometrical considerations. With the addition of B_T of a few gausses to the hexapole the flux lines are no longer closed and the wave is found to have considerably longer parallel wavelength and smaller perpendicular wavenumber compared with those without toroidal field. In the first branch (n = 0; the open circles) the wave moves towards the stable region of the drift wave with increasing the toroidal field. Similar variations are observed in the subsequent modes of waves with n = -1 and -2 (the rectangles and the triangles, respectively). Generally, plasma is unstable against the drift wave due to the inverse Landau damping and stabilized due to two possible mechanisms; [9,11] the first is contributed by the resonant electrons in the case of the frequency ω larger than the electron diamagnetic drift velocity ω_{*e} and the second is on account of ion Landau damping. The drift wave cannot be stabilized by good curvature in our toroidal hexapole especially for the microwave produced plasma $(T_e > T_i)$ because the parameter κR_c in the good region of the hexapole field is larger than the term $2(1 + T_i/T_e)$ by a factor of about 2 against the stability criterion[5] (see Fig. 3).

Measured wave characteristics in the plasma rest frame are summarized in Table II. The parallel phase velocity of the wave falls between the ion thermal velocity (4×10^5 cm/sec) and the electron thermal velocity (4.7×10^7 cm/sec). Also shown is the ratio of the parallel phase velocity to the electron thermal velocity $v_{\parallel}/v_{the}$. Except the differences in the frequency, the parallel wave length and the parallel phase velocity, the waves with and without toroidal field have similar properties suggesting that they belong to the same mode of waves. All these observations are consistent with the predictions for the density-gradient-driven drift wave.

E. Dispersion Relation

A comparison is made in Fig. 13 (a) between the theoretical perpendicular dispersion relation and the experimental one obtained by varying the toroidal field. The upper dotted line is the dispersion curve predicted qualitatively for a $\beta = 0$ plasma in the multipple configuration by Hastie and Taylor.[12] The solid curve is calculated for a $T_e = T_i$ plasma of a slab geometry by S. Yoshikawa.[11] The open circles and the solid dots in the figure represent the waves with and without toroidal field, respectively. The case is shown of the n = 0 mode. With the addition of B_T to the hexapole the wave jumps to a smaller $k_\perp \rho_i$ with a frequency drop. Further, the value of $k_\perp$ is found to decrease with increasing the toroidal field.

The experimental parallel dispersion curve of the waves is similarly obtained as shown in Fig. 13 (b). The solid dots represent the wave without toroidal field. With the addition of B_T to the hexapole the wave of the n = 0 mode jumps the minimum of $k_\parallel / \kappa$ (the open circles in the figure) and the value of $k_\parallel / \kappa$ is found to increase with increasing the toroidal field.

IV DISCUSSIONS

As shown in Table II the waves with and without toroidal field have similar properties consistent with those of the density-gradient-driven drift wave. The wave is considered to be a collisionless mode because the ratio of the electron-ion collision frequency (ν_{ei} = 690 kHz) to the frequency, ν_{ei}/ω is in the range of 1-5 with and without toroidal field[13] and the stabilization mechanism of poloidal modes is provided by ion Landau damping shown later.[14] The frequency drop with the addition of B_T to the hexapole is seen to be consistent with the observed decrease in $k_\perp$ on the perpendicular dispersion curve (see Fig. 13 (a)). The theoretical parallel dispersion curve is needed for a detailed discussion, but it is roughly approximated by $\omega \simeq k_\parallel v_s$, where v_s is the ion sound velocity (the dotted line in Fig. 13 (b)). The observed increase in the parallel wavelength is found to be qualitatively in agreement with the observed decreases in the frequency and the perpendicular wavenumber with the addition of B_T to the hexapole. These results indicate that the waves with and without toroidal field are the same mode of waves and are identified as the density-gradient-driven collisionless drift waves.

E. Dispersion Relation

A comparison is made in Fig. 13 (a) between the theoretical perpendicular dispersion relation and the experimental one obtained by varying the toroidal field. The upper dotted line is the dispersion curve predicted qualitatively for a $\beta = 0$ plasma in the multipple configuration by Hastie and Taylor.[12] The solid curve is calculated for a $T_e = T_i$ plasma of a slab geometry by S. Yoshikawa.[11] The open circles and the solid dots in the figure represent the waves with and without toroidal field, respectively. The case is shown of the n = 0 mode. With the addition of B_T to the hexapole the wave jumps to a smaller $k_\perp \rho_i$ with a frequency drop. Further, the value of $k_\perp$ is found to decrease with increasing the toroidal field.

The experimental parallel dispersion curve of the waves is similarly obtained as shown in Fig. 13 (b). The solid dots represent the wave without toroidal field. With the addition of B_T to the hexapole the wave of the n = 0 mode jumps the minimum of $k_\parallel / \kappa$ (the open circles in the figure) and the value of $k_\parallel / \kappa$ is found to increase with increasing the toroidal field.

IV DISCUSSIONS

As shown in Table II the waves with and without toroidal field have similar properties consistent with those of the density-gradient-driven drift wave. The wave is considered to be a collisionless mode because the ratio of the electron-ion collision frequency (ν_{ei} = 690 kHz) to the frequency, ν_{ei}/ω is in the range of 1-5 with and without toroidal field[13] and the stabilization mechanism of poloidal modes is provided by ion Landau damping shown later.[14] The frequency drop with the addition of B_T to the hexapole is seen to be consistent with the observed decrease in $k_\perp$ on the perpendicular dispersion curve (see Fig. 13 (a)). The theoretical parallel dispersion curve is needed for a detailed discussion, but it is roughly approximated by $\omega \simeq k_\parallel v_s$, where v_s is the ion sound velocity (the dotted line in Fig. 13 (b)). The observed increase in the parallel wavelength is found to be qualitatively in agreement with the observed decreases in the frequency and the perpendicular wavenumber with the addition of B_T to the hexapole. These results indicate that the waves with and without toroidal field are the same mode of waves and are identified as the density-gradient-driven collisionless drift waves.

B. Mode Transition of Poloidal Mode Number

As to the mode transition of poloidal mode number n we assume in the analogy of the results in the Q-machine[8,9] that one mode with a given n becomes dominant, within the limits of the linearized theory, if it has a larger growth rate than those of the other modes. By eliminating λ_θ from Eqs. (1) and (2), the geometrical condition for $\lambda_{\parallel}$ and $k_\perp$ is obtained as

$$\lambda_{\parallel}\left\{k_\perp + n\left(\frac{l_\theta}{L_0} + \frac{2\pi R\int R^{-1}dl_p/\int dl}{l_\theta}\right)\right\} = \frac{2\pi R\int R^{-1}dl_p}{l_\theta} \quad . \qquad (4)$$

The curves of Eq. (4) with n = 0, ±1, ±2, ... for a given toroidal field will be drawn on the ($\lambda_{\parallel}\kappa$, $k_\perp\rho_i$) plane, as shown in Fig. 14 for I_T = 3 A (the dot-dash-lines). Also shown in the figure are the stable and unstable regions of the density-gradient-driven collisionless drift wave and the contours lines of constant growth rate.[10] The first mode number n with the addition of B_T to the hexapole is expected from the curve to be n = 0 as observed in the experiment. According to Eq. (4) the group of curves with different mode number are shifted towards the left ordinate with increasing the toroidal field. Successive mode transitions of n = -1, -2, ... are predicted to occur with increasing the toroidal field which agree with the experimental results. The stabilization of each mode beyond a critical toroidal field is likely due to ion Landau damping,[9,11] because the ratio of the parallel phase velocity to the ion thermal velocity $v_{\parallel}/v_{thi}$ is found to decrease with increasing the toroidal field under the condition of $\omega < \omega_{*e}$ and to be about 5 near the transition region for the n = 0 mode as shown in Fig. 15. The observed critical ratio is in reasonable agreement with a thecretical value of 2.6.[9]

On the other hand, there are several difficulties to be solved. Firstly, the wave behaviours on the ($\lambda_{\parallel}\kappa$, $k_\perp\rho_i$) plane expected from the above assumption are shown in Fig. 14 by the open circles (the n = 0 mode) and the rectangles (the n = -1 mode) when the toroidal field is added to the hexapole. The behaviours of the waves with n = -1 differ considerably from the experimental results shown in Fig. 12 and the critical toroidal fields where mode transitions are predicted to occur (I_T = 2, 7, and 14 A) are smaller than the observed ones (I_T = 3, 22, and ~45 A) by a factor of 2-3. However, we believe that these discrepancies are ascribed mostly to the difference of the contour lines of constant growth rate referred[10]

from those in our plasmas. For example, the lines are known to be very sensitive to the temperature gradient ∇T_e in the long wavelength region ($k_\perp \rho_i \lesssim 1$)[5,15] as in the present experiment. Secondly, the correspondence of the observed wave amplitude shown in Fig. 11 (c) to the growth rate is not so good when the toroidal field is increased. This discrepancy may be partly due to the difference of the contour lines described above and partly due to lack of linearity of the observed waves since the waves are found to be in a state of large amplitude and sometimes of amplitude modulation.

In the above discussions we have neglected the effect of magnetic shear because the maximum shear parameter in the present experiment is 3.7×10^{-3} which is smaller than a theoretical value estimated from a criterion for the shear stabilization of the collisionless drift wave[16] at least by a factor of about 10. Experimentally, the wave amplitude is reduced to less than 3 % when the toroidal field of I_T = 300-400 A is superimposed on the hexapole field. This result is presumably related to shear stabilization.

In summary, we have observed the density-gradient-driven collisionless drift waves in the JAERI toroidal hexapole (JFT-1). The identification of the mode and the interpretation of mode transitions of poloidal mode number are made on the basis of the experimental results compared with the results predicted from linear theory of a slab geometry.

ACKNOWLEDGMENTS

It is a pleasure to thank Professor S. Yoshikawa for stimulating discussions and Dr. T. Dodo for valuable comments. We also wish to express our thanks to Dr. S. Mori and Dr. M. Yoshikawa who encourage this study.

from those in our plasmas. For example, the lines are known to be very sensitive to the temperature gradient ∇T_e in the long wavelength region ($k_\perp \rho_i \lesssim 1$)[5,15] as in the present experiment. Secondly, the correspondence of the observed wave amplitude shown in Fig. 11 (c) to the growth rate is not so good when the toroidal field is increased. This discrepancy may be partly due to the difference of the contour lines described above and partly due to lack of linearity of the observed waves since the waves are found to be in a state of large amplitude and sometimes of amplitude modulation.

In the above discussions we have neglected the effect of magnetic shear because the maximum shear parameter in the present experiment is 3.7×10^{-3} which is smaller than a theoretical value estimated from a criterion for the shear stabilization of the collisionless drift wave[16] at least by a factor of about 10. Experimentally, the wave amplitude is reduced to less than 3 % when the toroidal field of I_T = 300-400 A is superimposed on the hexapole field. This result is presumably related to shear stabilization.

In summary, we have observed the density-gradient-driven collisionless drift waves in the JAERI toroidal hexapole (JFT-1). The identification of the mode and the interpretation of mode transitions of poloidal mode number are made on the basis of the experimental results compared with the results predicted from linear theory of a slab geometry.

ACKNOWLEDGMENTS

It is a pleasure to thank Professor S. Yoshikawa for stimulating discussions and Dr. T. Dodo for valuable comments. We also wish to express our thanks to Dr. S. Mori and Dr. M. Yoshikawa who encourage this study.

REFERENCES

1. For reviews see, A. B. Mikhailovskii, in Reviews of Plasma Physics, edited by M. A. Leontovich (Consultant Bureau, New York, 1967), Vol. 3, p. 159; B. B. Kadomtsev, in Plasma Turbulence, (Academic Press, New York, 1965), p. 78; V. A. Krall, in Advances in Plasma Physics, edited by A. Simon and W. B. Thompson (Interscience Publishers, New York, 1968), Vol. 1, p. 153.
2. L. I. Rudakov and R. Z. Sagdeev, Zh. Eksp. Teor. Fiz. 37, 1337 (1959) [Soviet Phys. -JETP 10, 952 (1960)]
3. N. A. Krall and M. N. Rosenbluth, Phys. Fluids 6, 254 (1963).
4. L. V. Mikhailovskaya and A. B. Mikhailovskii, Zh. Tekh. Fiz. 33, 1200 (1963) [Soviet Phys.-Tech. Phys. 8, 896 (1964)] .
5. N. A. Krall and M. N. Rosenbluth, Phys. Fluids 8, 1488 (1965).
6. P. A. Rutherford and E. A. Frieman, Phys. Fluids 11, 569 (1968).
7. S. Tamura et al., in Proceedings of the Fourth International Conference on Plasma Physics and Controlled Nuclear Fusion Research, Madison, 1971, (International Atomic Energy Agency, Vienna, 1972), Vol. I, p. 75; S. Tamura et al., in Proceedings of the Fifth European Conference on Controlled Fusion, and Plasma Physics, Grenoble, August 1972, Vol. I, p. 94 and Vol. II, p. 240.
8. H. W. Hendel et al., Phys. Rev. Lett. 18, 439 (1967); H. W. Hendel et al., Phys. Fluids 11, 2426 (1968).
9. P. A. Politzer, Phys. Fluids 14, 2410 (1971).
10. P. Brossier, EURATOM-Centre à l'Energie Atimique Report No. EUR-CEA-FC-565 (1970).
11. S. Yoshikawa, in Methods of Experimental Physics, edited by H. R. Griem and B. Lovberg (Academic Press, New York, 1970), Vol. 9, Part A, p. 319.
12. R. J. Hastie and J. B. Taylor, Plasma Phys. 13, 265 (1971).
13. D. K. Bhadra, Phys. Fluids 14, 977 (1971).
14. See Ref. 8; F. F. Chen et al., in Proceedings of the Third International Conference on Plasma Physics and Controlled Nuclear Fusion Research, Novosibirsk, 1968, (International Atomic Energy Agency, Vienna, 1969), Vol. I, p. 625; R. E. Rowberg and A. Y. Wong, Phys. Fluids 13, 661 (1970).
15. P. Brossier et al., Nucl. Fusion 12, 453 (1972).
16. L. V. Mikhailovskaya and A. B. Mikhailovskii, Nucl. Fusion 3, 28

(1963); J. D. Jukes, Phys. Fluids 7, 1468 (1964); P. H. Rutherford and E. A. Frieman, Phys. Fluids 10, 1007 (1967); L. D. Pearlstein and H. D. Bers, Phys. Rev. Lett. 23, 220 (1969); M. Mishin, Zh. Eksp. Teor. Fiz. 59, 2252 (1970) [Soviet Phys.-JETP 32, 1218 (1971)].

TABLE I Machine parameters

Major radius (cm)	43.5
Average hexapole field on (G)	$B_P = \oint dl_P / \oint dl_P / B_P = 460$
Length of the closed flux line (cm)	$L_0 = \oint dl_P = 80$
Toroidal field near the minor axis (G)	0-90
Maximum shear parameter	$\textcircled{H} = 1/\kappa L_s = 3.7 \times 10^{-3}$

TABLE II Measured wave characteristics in the plasma rest frame

I_T (A)	0	2-80
Frequency (kHz)	59-85	19-39
Perpendicular wavelength (cm)	2.0-3.2	3.6-8.7
Perpendicular phase velocity $v_\perp$ (10^5 cm/sec)	1.2-2.7	0.7-3.4
ω / ω_{*e}	0.7-0.9	0.5-0.8
$k_\perp \rho_i$	0.21-0.3	0.09-0.18
Propagation	Electrons	Electrons
Parallel wavelength (cm)	80	89-749
Parallel phase velocity $v_\parallel$ (10^6 cm/sec)	4.7-6.8	1.7-29
$v_\parallel / v_{the}$	0.1-0.14	0.04-0.6
Phase difference $\Delta_\psi = \psi(\tilde{n}) - \psi(\tilde{\phi})$ (deg)	71 ± 27	94 ± 51

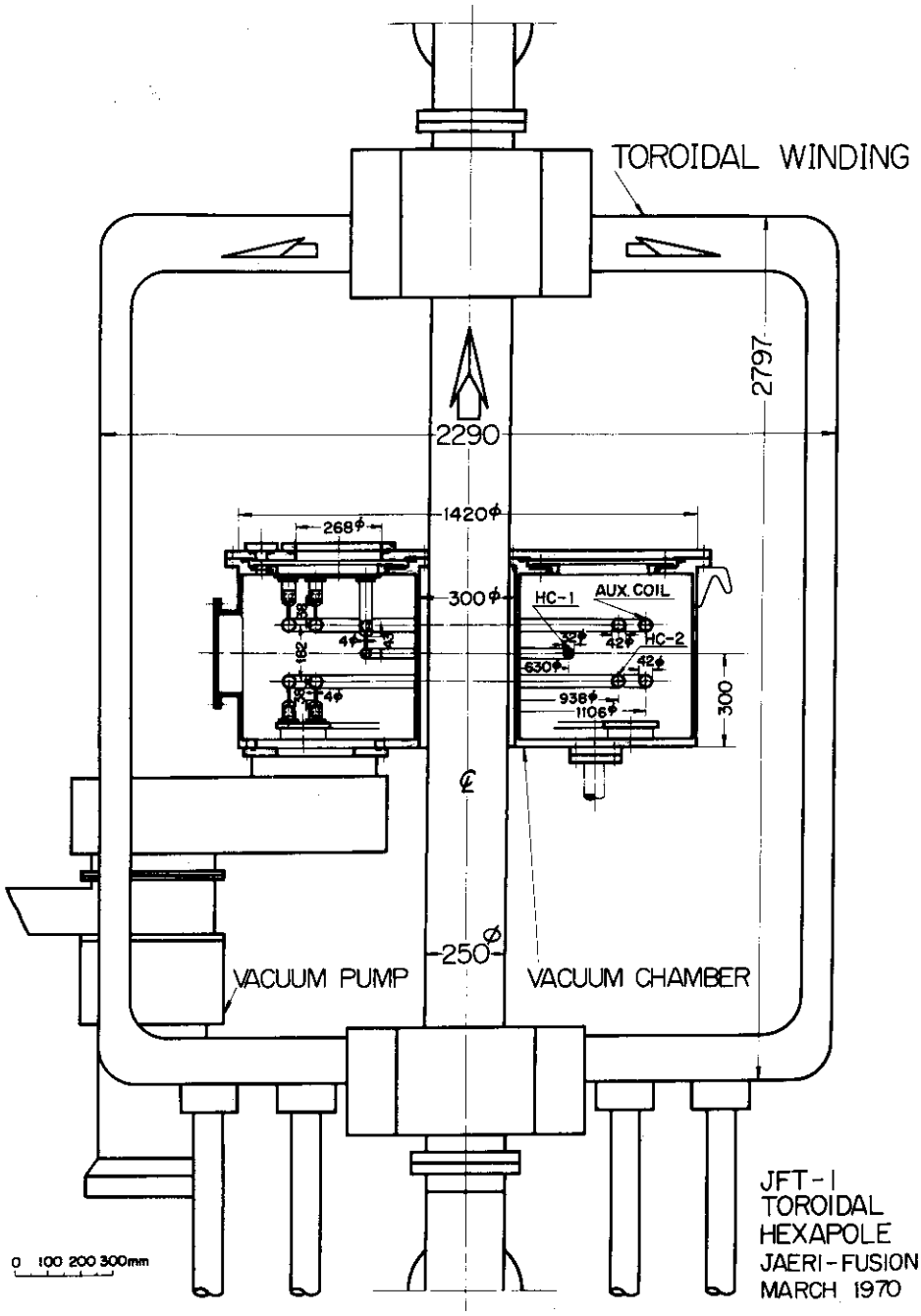

Fig. 1. Cross-sectional view of the JAERI toroidal hexapole (JFT-1).

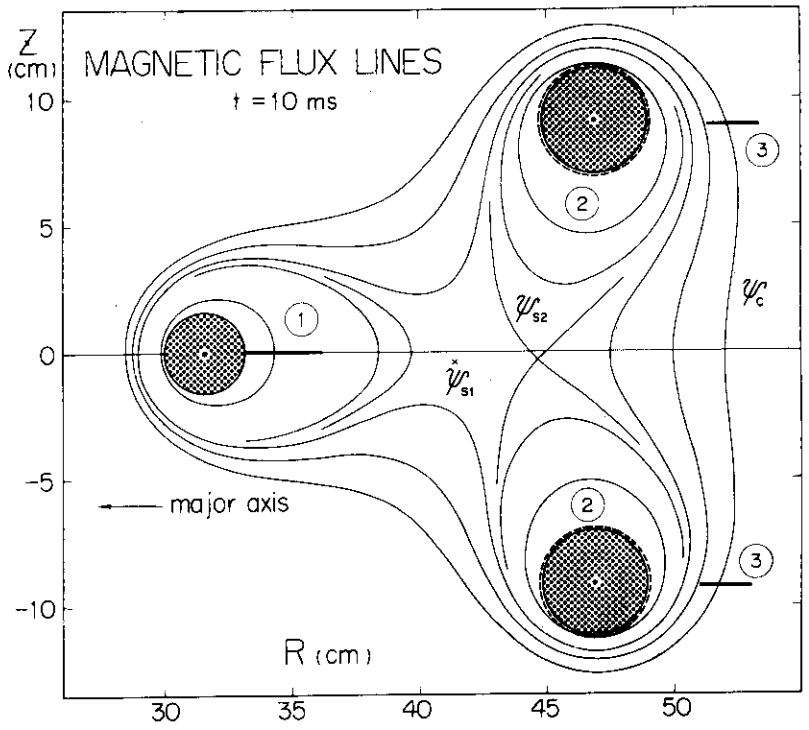

Fig. 2. Flux pattern of the hexapole. Also shown are the limiters (1 and 3) used as particle loss detectors and the outer hoop loss detectors (2).

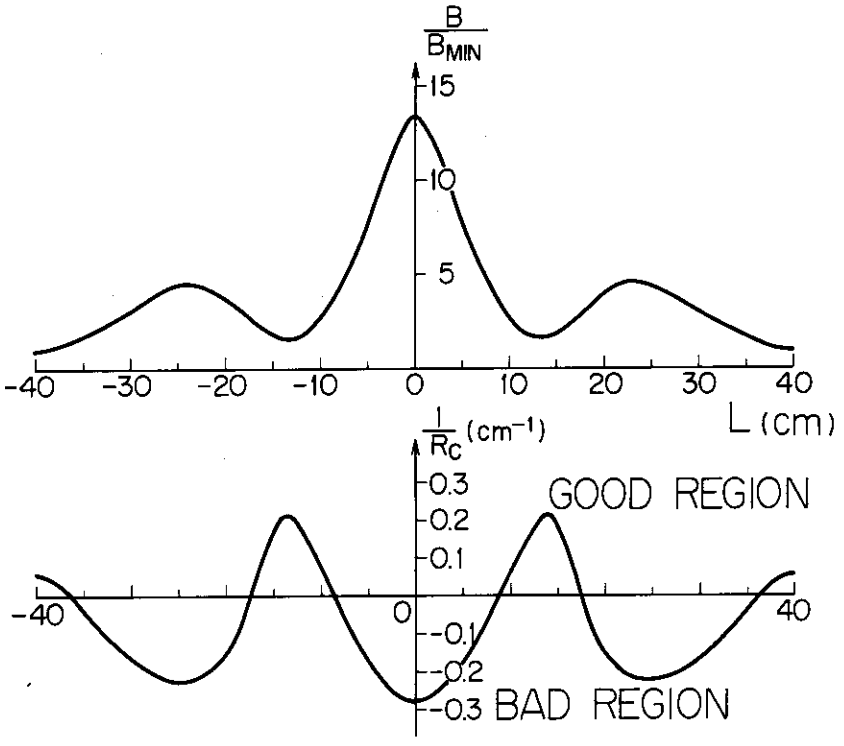

Fig. 3. Mirror ratio B/B_{MIN} and reciprocal of the radius of curvature of the magnetic field along the typical flux line which passes through the point with the coordinates (40, 5.5) in Fig. 2. The distance L is measured along the flux line from the nearest point to the symmetric axis.

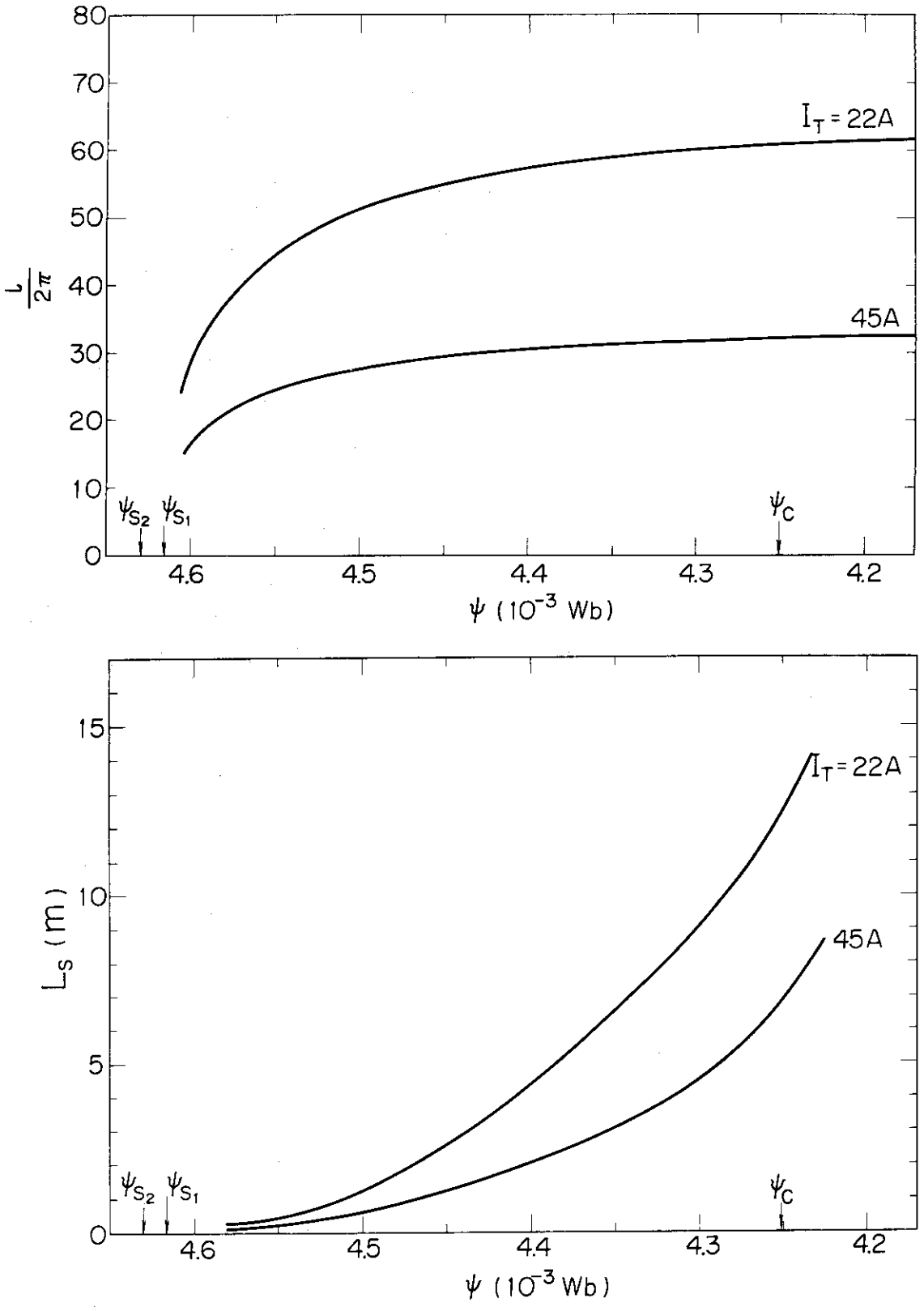

Fig. 4. (a) Rotational tranceform angle $\iota / 2\pi$ as a function of the flux ψ for two toroidal fields of I_T = 22 and 45 A. (b) Average shear length L_S as a function of the flux ψ for two toroidal fields of I_T = 22 and 45 A.

200 μsec/div

(a)

10 μsec/div

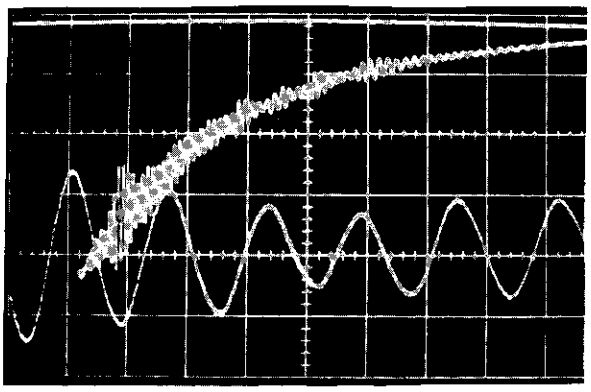

200 μsec/div

(b)

50 μsec/div

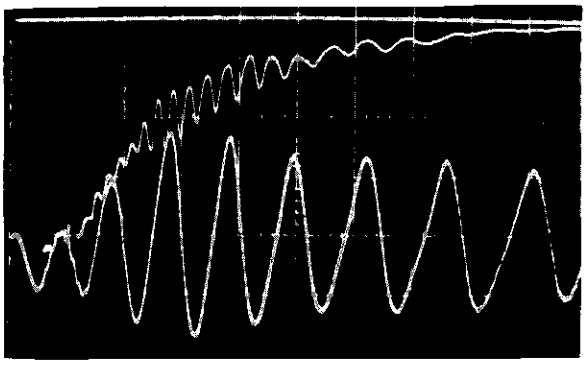

Fig. 5. Oscilloscope traces of ion saturation current are shown (a) with no toroidal field and (b) with toroidal field of I_T = 10 A. The upper traces (turned upside-down) are triggered just after the microwave heating pulse is turned off and the lower traces are at 400 μ sec after the pulse.

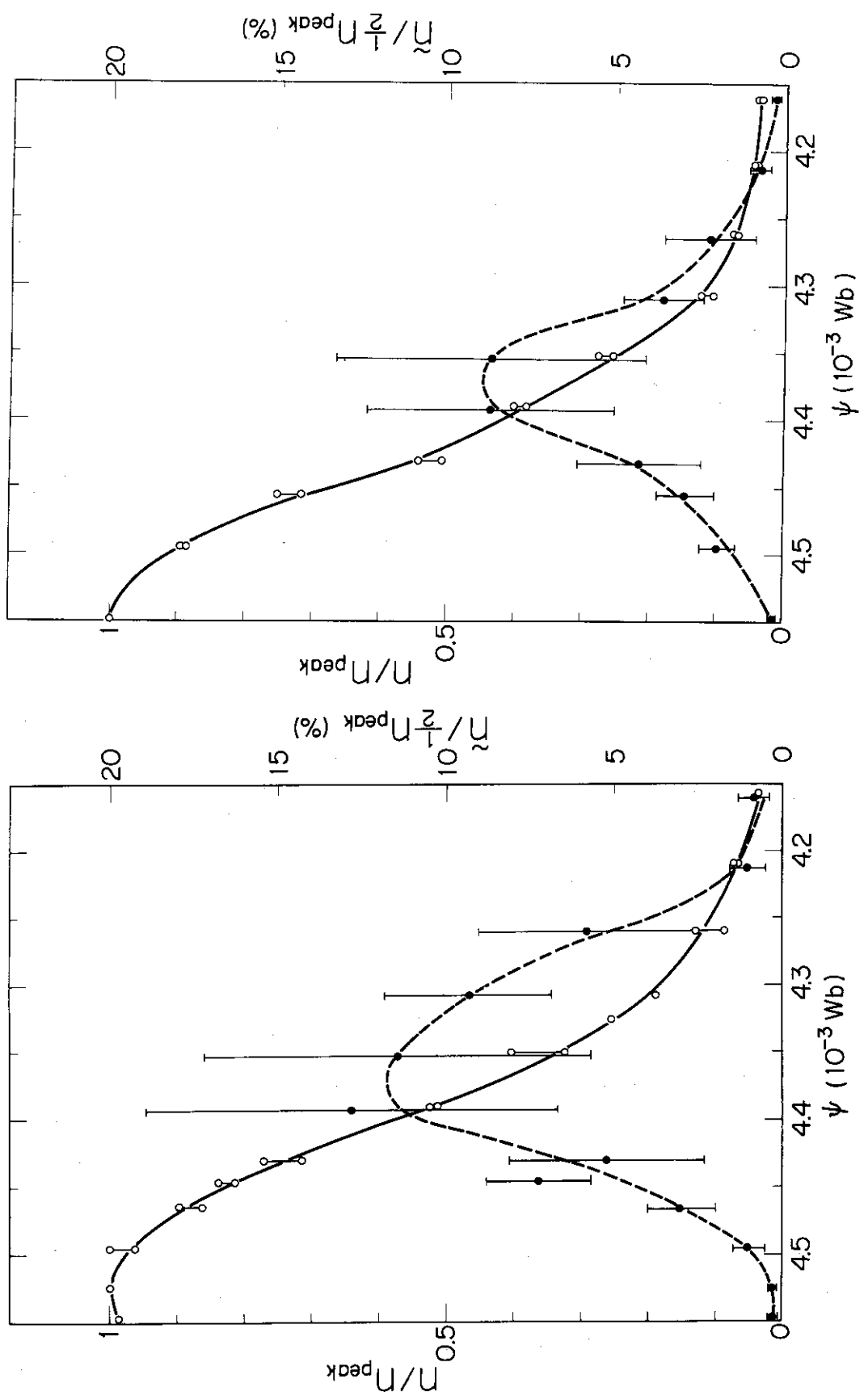

Fig. 6. Radial density profile (the solid line) and the localization of the wave amplitude (the dotted line) versus the flux ψ. (a) With no toroidal field, (b) with toroidal field of I_T = 10 A.

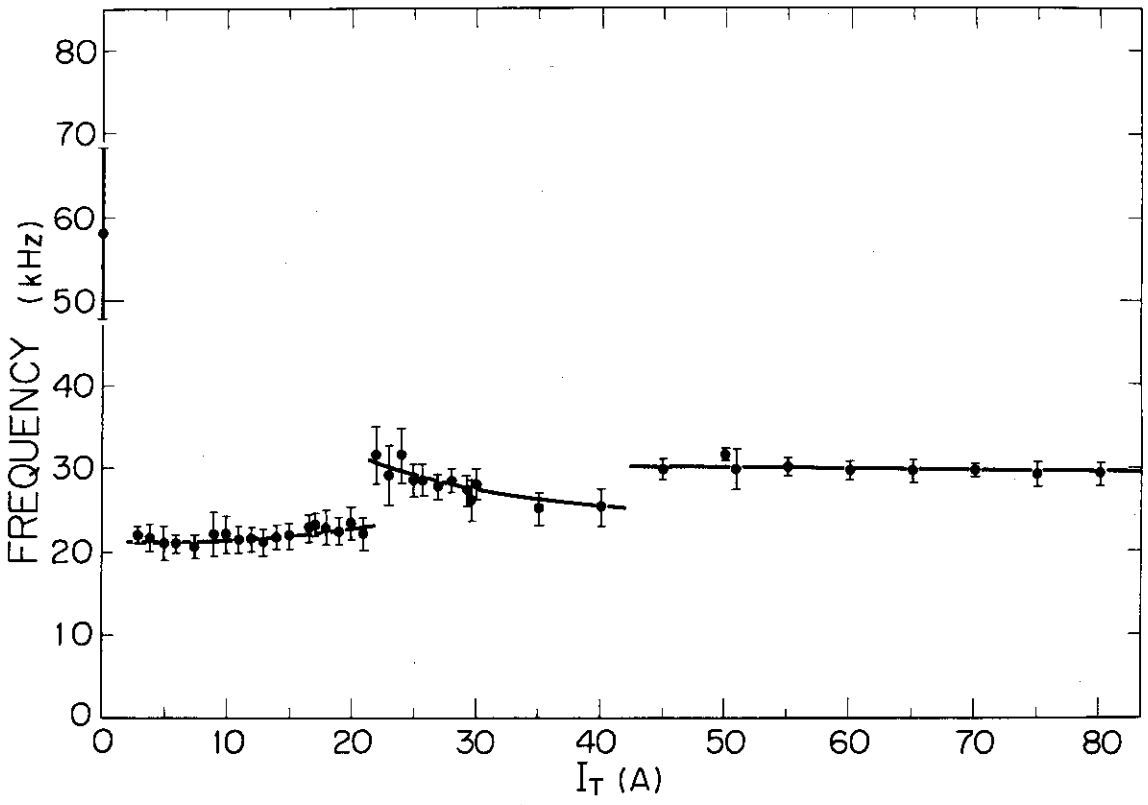

Fig. 7. Frequency of the wave in the laboratory frame as a function of toroidal field.

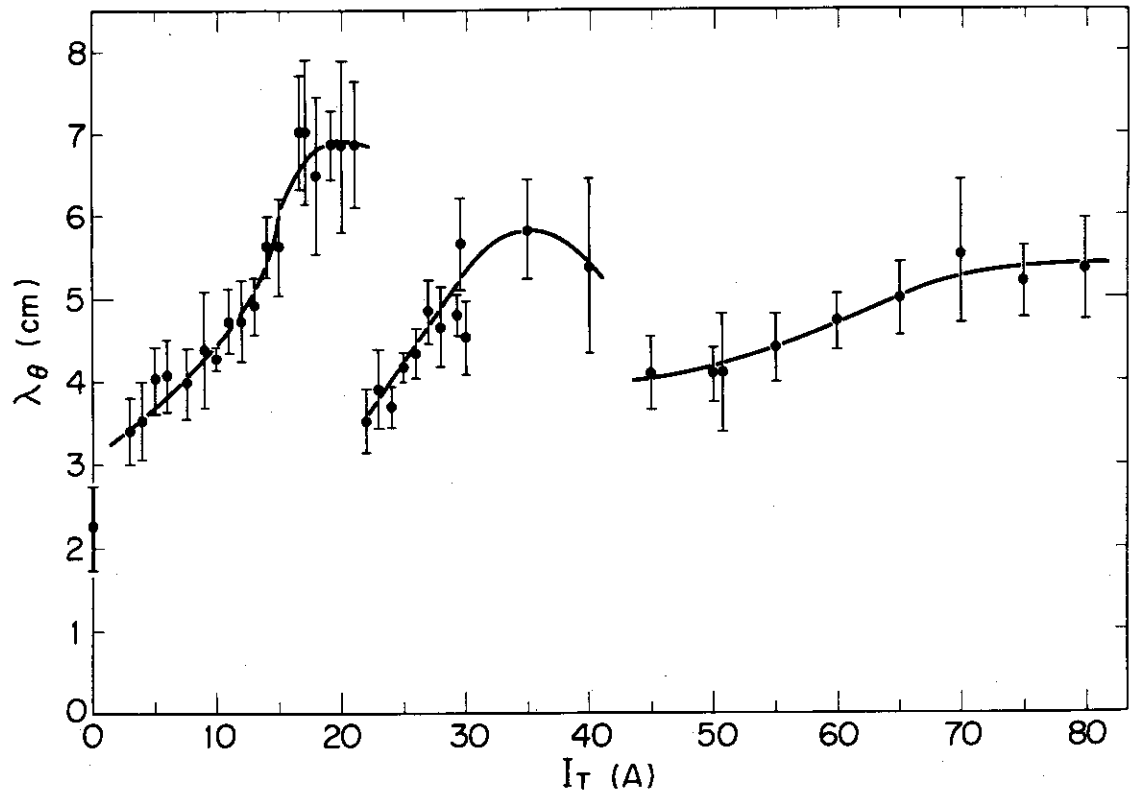

Fig. 8. Azimuthal wavelengths as a function of toroidal field.

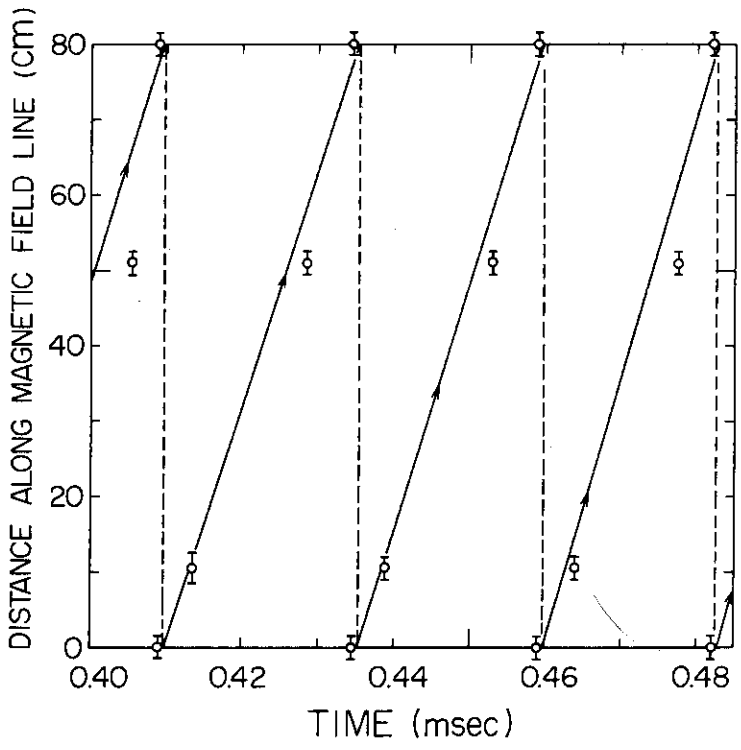

Fig. 9. Positions of the maxima of the waveform shown in Fig. 5 are ploted as a function of time delay for three positions along the same flux line.

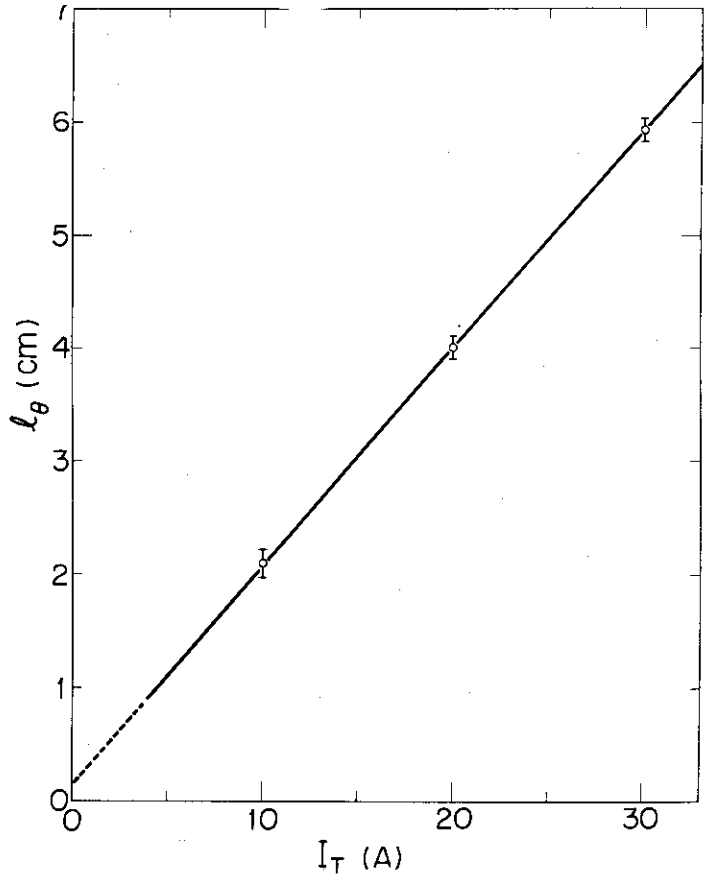

Fig. 10. Pitch length ℓ_θ of the flux line as a function of toroidal field.

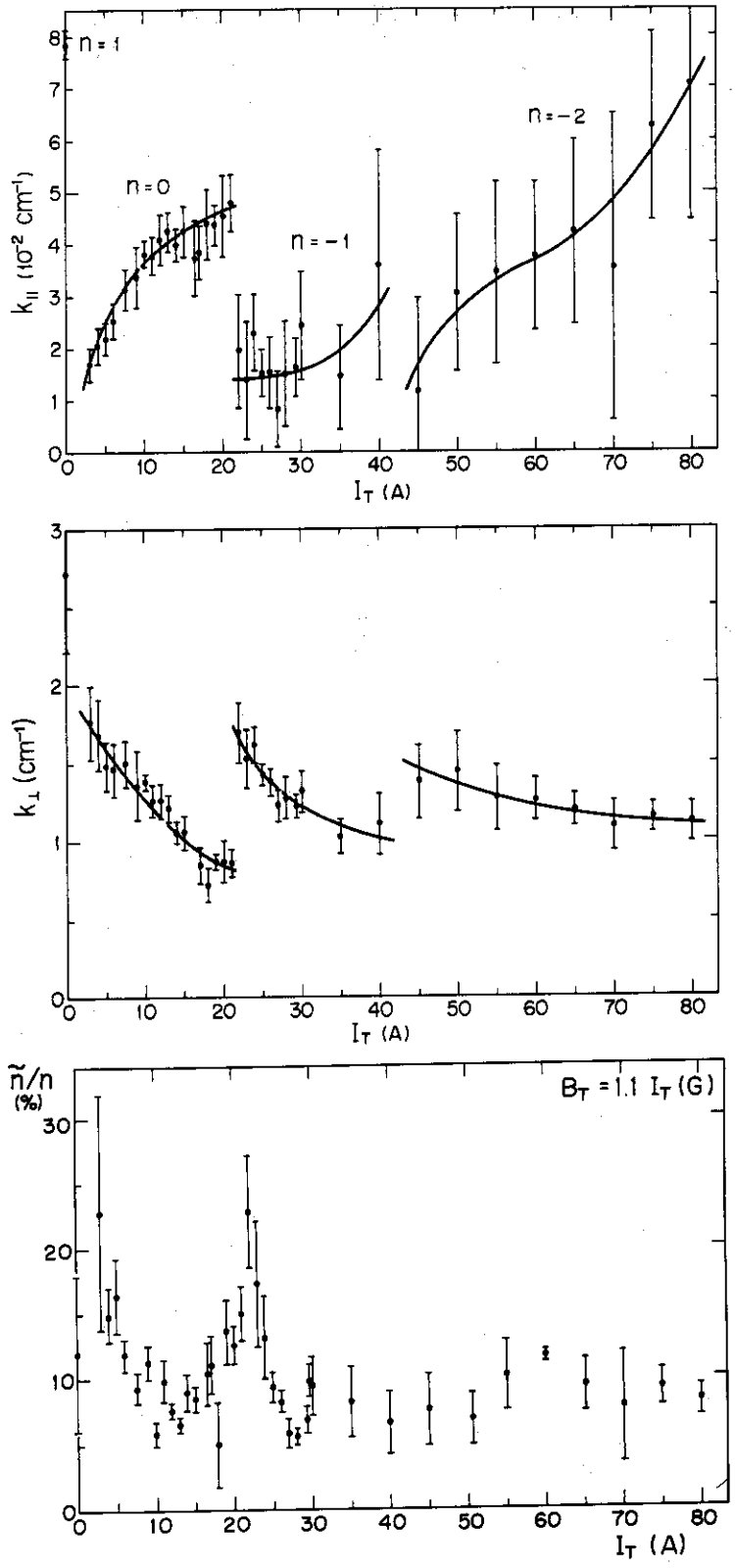

Fig. 11. Parallel and perpendicular wavelengths versus toroidal field are shown in (a) and (b), respectively. The wave amplitude versus toroidal field is shown in (c).

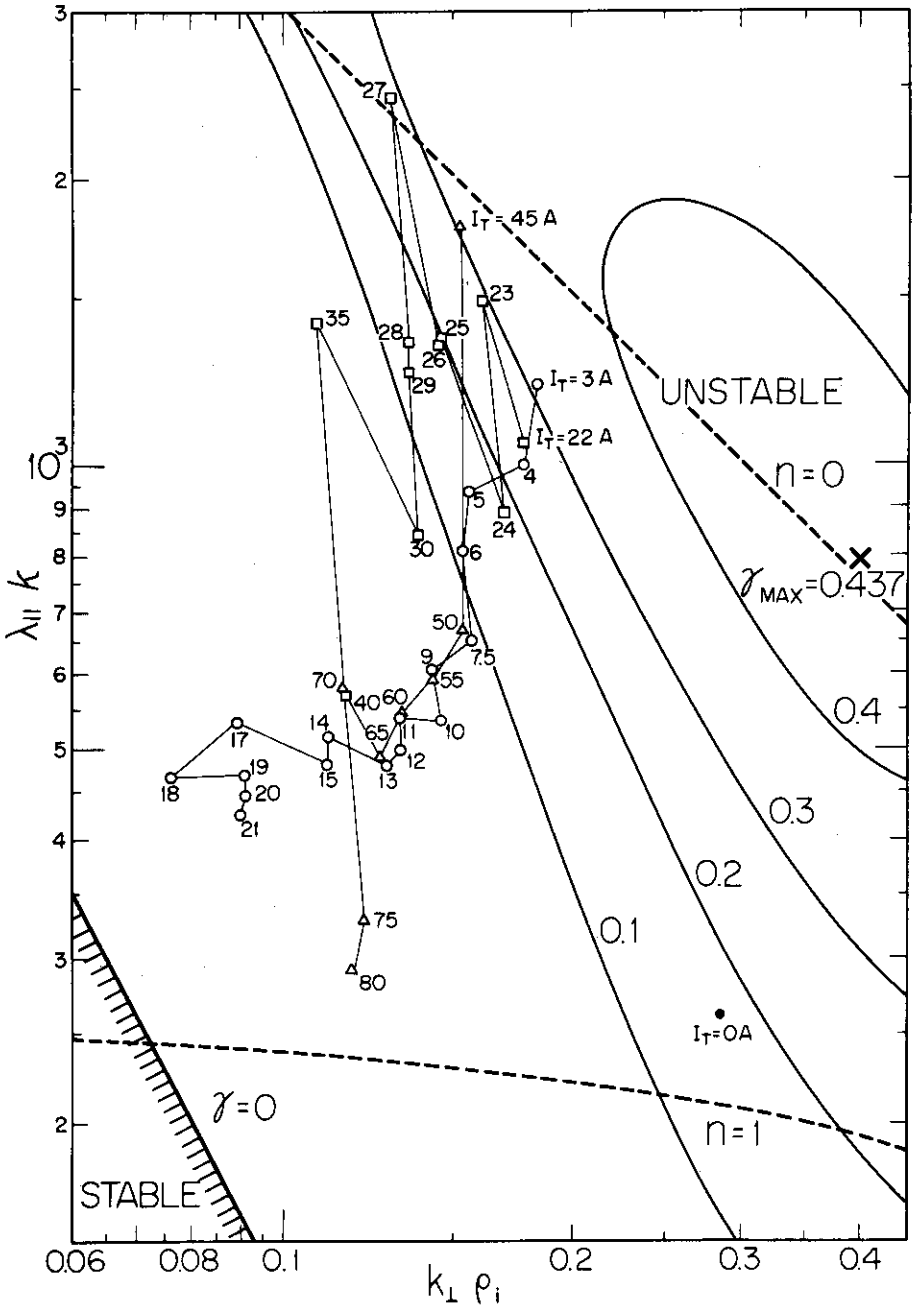

Fig. 12. Wave behaviors on the ($\lambda_{11}\kappa$, $k_\perp \rho_i$) plane when the toroidal field is increased from I_T = 0 A. Also partly shown are the stable and unstable regions of the collisionless drift waves and contour of constant growth rates, $\gamma = \omega_1 / \kappa v_{thi}$ for T_e/T_i = 10 and ∇T_e = 0, where ω_1 is the imaginary part of the frequency ω and v_{thi} is the ion thermal velocity.[10] The dotted lines are calculated from Eq. (4) for I_T = 2 A with n = 0 and -1, respectively.

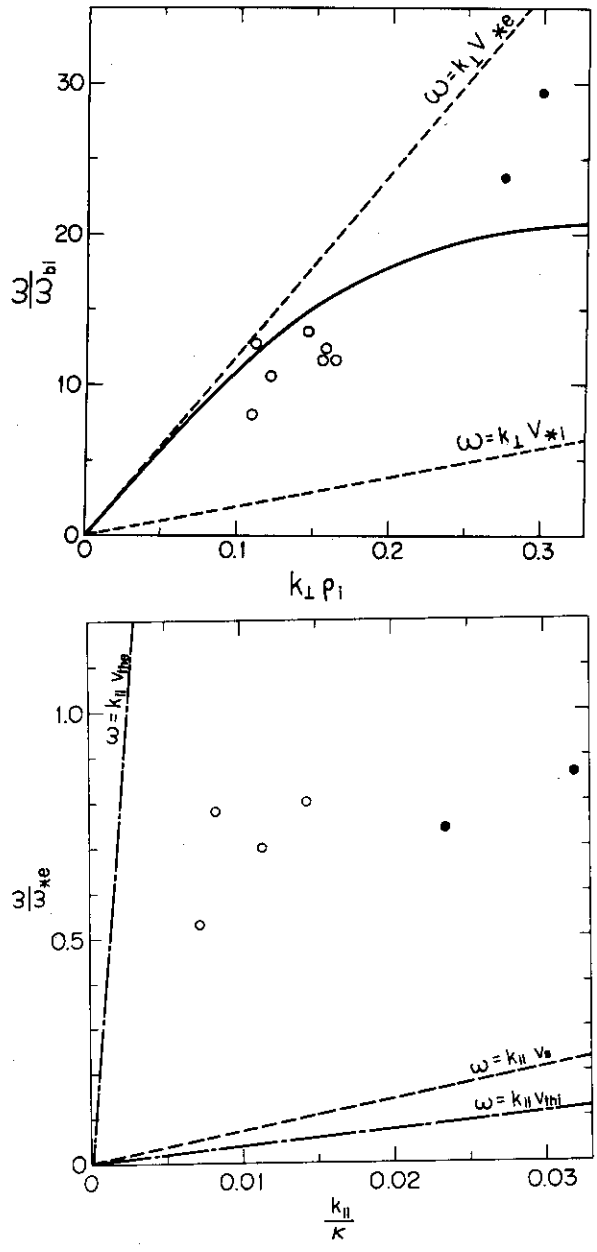

Fig. 13. (a) Perpendicular dispersion relation. The open circles and solid dots represent the n = 0 mode and the n = 1 mode, respectively. The upper dotted line is the dispersion curve predicted qualitatively for a $\beta = 0$ plasma in the multipole configuration[12] and the solid curve is calculated for a $T_e = T_i$ plasma of a slab geometry.[11] Here, the ion bounce frequency ω_{bi} is defined as $\omega_{bi} = \pi v_{thi}/L_0$. (b) Parallel dispersion relation. The dotted line is the velocity of the ion sound wave.

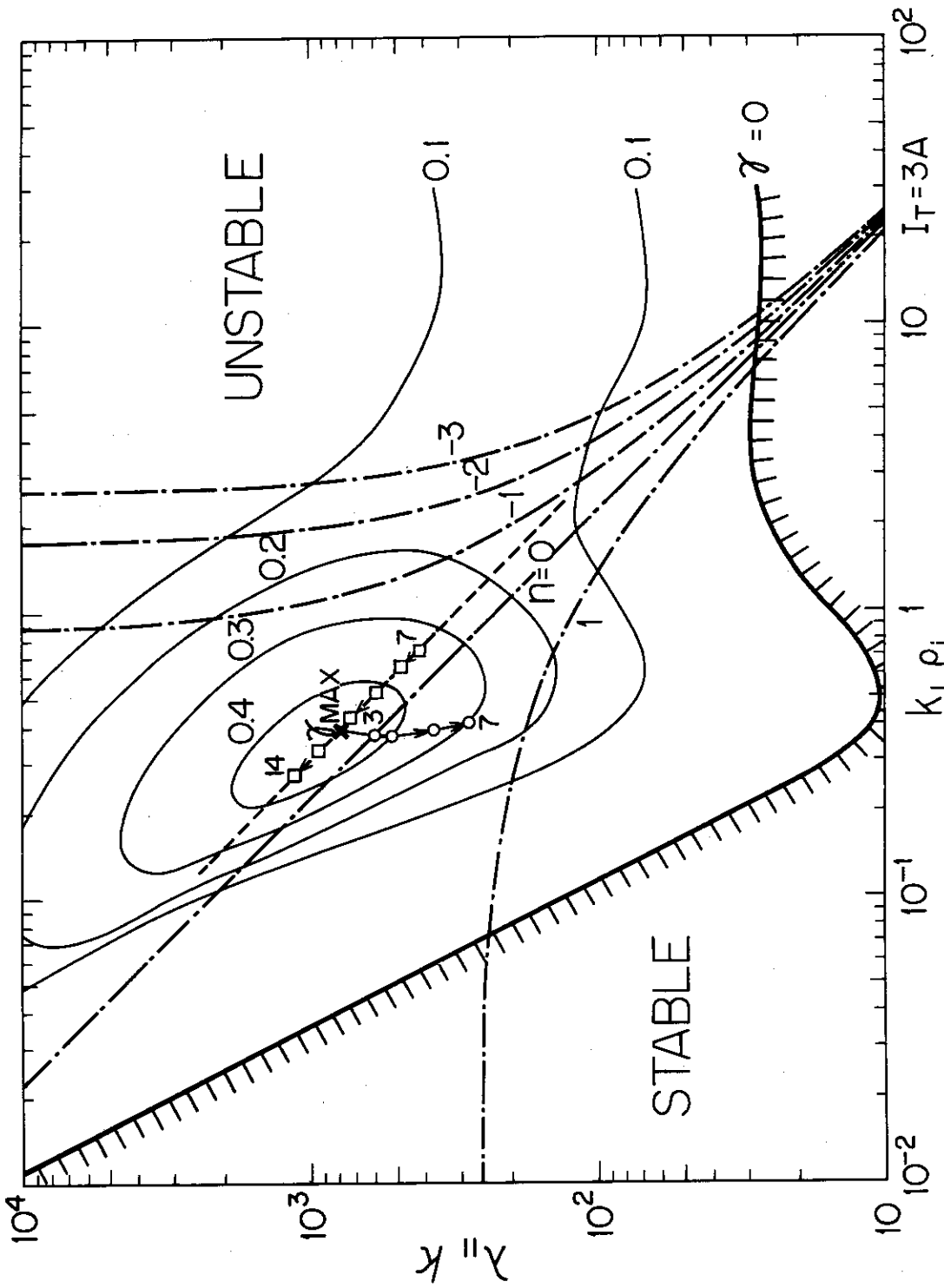

Fig. 14. Expected wave behaviours and the curve of Eq. (4) with n = 0, ±1, -2, and -3 for I_T = 3 A. The open circles and the rectangles represent the waves with n = 0 and -1, respectively. Also shown are the contour lines of constant growth rates of the drift waves.[10]

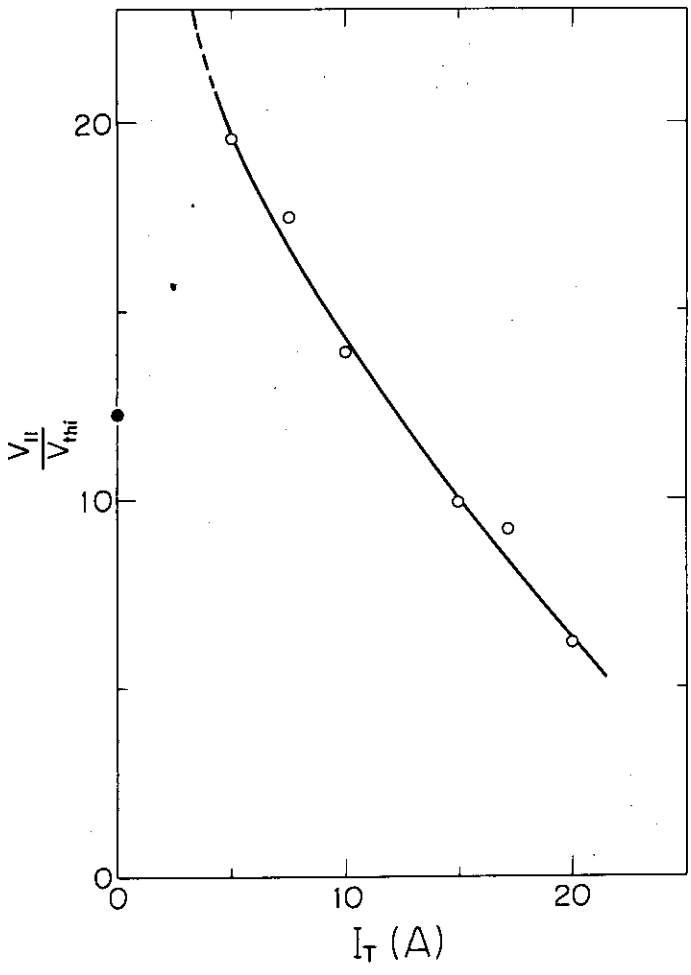

Fig. 15. Ratio of the parallel phase velocity to the ion thermal velocity for the n = 1 mode (the solid dot) and the n = 0 mode (the open circles) as a function of toroidal field.